
Role of vacancies and impurities in the ferromagnetism of semiconducting CaB_6

KALOBARAN MAITI,^(a)

Department of Condensed Matter Physics and Materials Science, Tata Institute of Fundamental Research, Homi Bhabha Road, Colaba, Mumbai - 400005, INDIA

PACS 75.50.Pp – Magnetic properties and materials; Magnetic semiconductors

PACS 71.55.-i – Electronic structure of bulk materials; Impurity and defect levels

PACS 75.10.Lp – Magnetic properties and materials; Band and itinerant models

Abstract. - We investigate the influence of impurities and vacancies in the formation of magnetic moment in CaB_6 using full potential *ab initio* band structure calculations. CaB_6 is found to be a band insulator with a band gap of about 0.2 eV. The calculated results indicate that carbon and oxygen substitution in boron sublattice, usually expected as impurity in low purity borons, do not play significant role in the local moment formation. Boron vacancy in the boron sublattice, on the other hand, leads to the formation of an impurity band in the vicinity of the Fermi level, which exhibit finite exchange splitting and magnetic moment. All these results provide remarkable representation of the experimental results. This finding of the role of vacancies in the sublattice responsible for electronic conduction is an important revelation in the understanding of ferromagnetism in the diluted electron system.

Introduction. – Study of ferromagnetism in diluted electron systems (diluted magnetic semiconductors, [1] hexaborides [2] etc.) having high Curie temperature, T_C has seen an explosive growth in the recent times due to its potential applications in the spin based technology. It is believed that in these systems, the spin degrees of freedom can be used for data storage and data processing in addition to the use of charge that is used in the present day technology. Despite numerous studies, the primary concern of the origin of ferromagnetism in these systems is still unresolved. While this is a fundamental issue, it is expected to be instrumental for tailoring new materials those are necessary for the further development in technology.

In this regard, the discovery of unusual ferromagnetism in hexaborides, MB_6 ($M = \text{Ca}, \text{Sr}, \text{Ba}$ etc.) and in La-doped CaB_6 ($T_C \geq 600$ K) is unique and unusual. High purity CaB_6 is a band insulator. [2–4] A small amount of impurity leads to ferromagnetism in CaB_6 . While this fact is somewhat similar to the diluted magnetic semiconductors, the unique feature in hexaborides is that the magnetization appears despite the absence of any magnetic element in the composition of these compounds. Thus, the origin of magnetic moment and hence, ferromagnetism is puzzling.

Several studies have been performed attributing the ferromagnetism to the polarization of low density conduction electrons, [2, 5] excitons formed by the doped holes, [6] magnetic impurity due to the crucibles used for sample preparation, [7] impurities in the boron sub-

^(a)Electronic address: kbmaiti@tifr.res.in

lattice [8] *etc.* A recent photoemission study [9] reveals the presence of weakly localized states in the vicinity of the Fermi level, ϵ_F in the ferromagnetic CaB_6 while it is absent in the paramagnetic LaB_6 . [10] These studies [8,9] show that ferromagnetism in hexaborides may not be extrinsic arising due to the magnetic impurities as signature of such elements was not found in the ferromagnetic compositions. Thus, unlike diluted magnetic semiconductors, the weak local moment in this system may be related to the introduction of partial local character in the impurity states in the vicinity of Fermi level. However, the origin and character of such localized states are far from understood.

In this letter, we report our results on the influence of impurities in the electronic structure of CaB_6 using state-of-the-art full potential *ab initio* band structure calculations. We observe that the impurity contributions due to oxygen and carbon at the boron sites do not play significant role in the magnetic moment formation. On the other hand, the boron vacancy leads to the formation of distinct impurity feature in the vicinity of the Fermi level. The magnetic moment of these features in the spin polarized calculations are remarkably similar to that found experimentally.

Computational details. – CaB_6 forms in cubic structure with the space group $Pm3m$ and lattice constant $a = 4.152 \text{ \AA}$. [11] In order to introduce impurities in the B-sublattice, we have doubled the unit cell along one axis. The unit cell used for calculation is shown in Fig. 1. We have replaced B12 shown in the figure by C or O impurities separately, which introduces one impurity among 12 borons (8.3% impurity in one formula unit). Vacancies in the B-sublattice are introduced by removing B12. This allows to introduce 8.3% defects in the B-sublattice. Due to the limitation in computational facilities, larger unit cell could not be considered, which could allow even lower substitutional levels. Although the experimental cases correspond to somewhat lower degree of impurities, we believe that this model provides a good representation of the experimental cases to find the trend.

Band structure calculations were carried out using full potential linearized augmented plane wave method within the local spin density approximations (LSDA) using WIEN2k software. [13] The energy convergence was fixed to $\Delta E < 0.7 \text{ meV/fu}$ (fu = formula unit) and charge convergence achieved was $\Delta Q < 10^{-3}$ electronic charge/fu. In order to achieve the convergence 1000 k points were considered within the first Brillouin zone.

Results and Discussions. – The calculated density of states (DOS) corresponding to CaB_6 , $\text{CaB}_{5.5}\text{O}_{0.5}$ and $\text{CaB}_{5.5}\text{C}_{0.5}$ are shown in Fig. 2. The total density of states (TDOS) in CaB_6 exhibit a gap of about 0.2 eV at the Fermi level, ϵ_F (denoted by zero in the energy scale) indicating a band insulating phase in the ground state. The energy range -9 eV to -6 eV is primarily contributed by B $2s$ states (not shown here to maintain clarity in the figure) and the energy bands between -6 eV to ϵ_F have dominant B $2p$ character (see Fig. 2(c)). Ca $3d$ bands appear above ϵ_F with negligible contribution in the occupied part. A rescaling of the Ca $3d$ partial density of states (PDOS) by 30 times (shown by shifting along the y-axis in Fig. 2(b)) reveals that the energy distribution of Ca $3d$ states is strikingly similar to that observed for B $2p$ states in Fig. 2(c). This indicates significant covalency between Ca $3d$ and B $2p$ states.

The C or O substitution leads to a large shift (by more than 2 eV) of the $2p$ bands towards higher binding energies. This is expected as the total electron count in C and O is more than that in B. Hence, the Fermi level is expected to shift towards higher energies. Subsequently, the energy range near the lower energy tail of the Ca $3d$ bands becomes more intense and partially populated leading the ground state to a metallic phase. The DOS near ϵ_F is weak and flat in the C substituted compound. O substitution generates relatively larger contribution in the vicinity of ϵ_F along with a dip at ϵ_F and a small but sharp feature at about -0.5 eV.

The shift of the Ca $3d$ PDOS appear to be much smaller than that observed for B $2s$ and $2p$ PDOS. The rescaled Ca $3d$ PDOS in the lower energy region exhibit DOS distribution similar to that observed for B $2s2p$ states. The separation between the B $2p$ PDOS peak

and Ca 3d PDOS peak enhances by about 1 eV in the substituted compounds indicating signature of stronger hybridization. C 2p and O 2p PDOS looks significantly different from the distribution observed in B 2p and Ca 3d cases.

In order to investigate the influence of these features in the ferromagnetic ground state, we have calculated the ground state energies and magnetic moments for the same lattice within LSDA. We find that the difference between the total energies corresponding to non-magnetic and ferromagnetic solutions is less than the error bar considered for convergence criteria. The magnetic moment at each B and Ca site is $\sim 10^{-3} \mu_B$ per atom or lower. The magnetic moment centered at the C and O sites are $0.0036 \mu_B$ per substitution and $0.007 \mu_B$ per substitution, respectively. The total magnetic moment is found to be $< 0.005 \mu_B/fu$. The calculations for CaB₆ also exhibit similar scenario. All these results suggest that the C or O impurities at the boron sites do not have significant influence in deriving the magnetic moment in this system. The features in the vicinity of ϵ_F observed in all these cases are very different from those observed spectroscopically. [9]

It is thus evident that the magnetic moment observed in CaB₆, although weak, has different origin. We now turn to case of influence of vacancy in the electronic structure. Removal of B12 from the unit cell introduces 8.3% vacancy in one formula unit. The calculated DOS for this case is compared with the results of CaB₆ in Fig. 3. The DOS in the energy range away from ϵ_F (below -2 eV energy) remains almost similar to the results of CaB₆. Interestingly, the DOS in the vicinity of ϵ_F exhibit remarkable spectral weight redistribution. The DOS between 0 to -2 eV energies vanishes and a new energy band appears at ϵ_F (between -1 to +1 eV). We term this new energy band formed due to the boron vacancy in the boron sublattice as an *impurity band*. The electronic states corresponding to this *impurity band* are sufficiently itinerant having a bandwidth close to 2 eV and is partially filled, which indicates that the ground state is metallic.

Although the dominant contributions of the Ca 3d band in CaB_{5.5} appears in the same energy range as that of CaB₆, the low energy contributions in the vicinity of ϵ_F exhibit redistributions similar to the B 2p states. The dominant contribution in the impurity band comes from the 2p electronic states corresponding to borons around the vacancy site (B7 - B11) as shown in Fig. 3(d). The occupied part is primarily contributed by (B8 - B11) and contributions from B7 appears largely above ϵ_F .

The total energy for the ferromagnetic solution in this case also found to be close to that for the non-magnetic solutions; the energy difference is smaller than the convergence limit as observed in other cases. Interestingly, the magnetic moment in this case is found to be significantly larger than all the previous cases. The magnetic moment centered at B7 site and other four boron sites (B8 - B11) are $0.023 \mu_B$ and $0.003 \mu_B$ respectively. The magnetic moment at all the other sites are very small. The total magnetic moment is found to be $0.018 \mu_B/fu$, which is almost identical to that found experimentally. [12]

In Fig. 4, we show the calculated spin polarized DOS. It is evident that the exchange splitting is not distinctly visible in TDOS and Ca 3d partial DOS (PDOS). However, the 2p contributions from B7 and (B8 - B11) in the *impurity band* exhibit signature of finite exchange splitting. The splitting is maximum (~ 0.25 eV) in the case of B7 (see Fig. 4(b)). This is also manifested in the magnetic moment. This indicates that the 2p electronic states corresponding to B7 site have significant local character and play a key role in the ferromagnetism of these materials.

All the above results are remarkably consistent with the experimental observation of the 2p character of the impurity feature in the high resolution photoemission study [9] and the observation of the strong dependence of magnetic moment on defects. [12] The magnetism involving 2p electrons has been predicted in other systems such as C impurities in BN nanotubes. [14] Oxygen vacancy induced ferromagnetism has also been observed in d^0 oxides. [15] In this study, we observe that the C and O impurities do not play significant role in magnetic moment formation in CaB₆. The defects states due to the B vacancy form an *impurity band* in these systems. The *impurity band* has significant bandwidth to ensure

itineracy of the associated electrons and local character that plays the dominant role in determining the magnetic moment. These results, thus, provide an important input in the understanding of magnetism of these interesting materials. We hope that this will help to initiate further studies in this direction that is necessary to design and fabricate new materials of potential technological importance.

Conclusions. – In summary, we have investigated the origin of magnetic moment formation in CaB₆ using state-of-the-art full potential band structure calculations. CaB₆ is found to be a band insulator with a band gap of about 0.2 eV. Introduction of carbon or oxygen leads to a shift of the Fermi level towards higher energies. In these cases the ground state is metallic. The Ca 3*d* and B 2*p* hybridization strength is found to increase due to such substitutions. No influence of C or O substitution was observed in the formation of magnetic moment.

Introduction of vacancy in the boron sublattice leads to the formation of an *impurity band* in the vicinity of the Fermi level. Such impurity states have B 2*p* character consistent with the experimental observations and are located close to the vacancy site. The exchange splitting of these states is found to be finite leading to a magnetic moment that is consistent with the experimental results. These results suggest that the boron vacancy plays the key role in ferromagnetism in these diluted electron systems.

REFERENCES

- [1] DIETL T., OHNO H., MATSUKURA F., CIBERT J. and FERRAND D., *Science*, **287** (2000) 1019.
- [2] YOUNG D.P., HALL D., TORELLI M.E., FISK Z., SARRAO J.L., THOMPSON J.D., OTT H.-R., OSEROFF S.B., GOODRICHK R.G. and ZYSLER R., *Nature*, **397** (1999) 412.
- [3] VONLANTHEN P., FELDER E., DEGIORGI L., OTT H.R., YOUNG D.P., BIANCHI A.D. and FISK Z., *Phys. Rev. B*, **62** (2000) 10076.
- [4] OTT H.R., GAVILANO J.L., AMBROSINI B., VONLANTHEN P., FELDER E., DEGIORGI L., YOUNG D.P., FISK Z. and ZYSLER R., *Physica (Amsterdam)*, **281B & 282B** (2000) 423.
- [5] CEPERLEY D., *Nature (London)*, **397** (1999) 386.
- [6] ZHITOMIRSKY M.E., RICE T.M. and ANISIMOV V.I., *Nature (London)*, **402** (1999) 251; ZHITOMIRSKY M.E. and RICE T.M., *Phys. Rev. B*, **62** (2000) 1492.
- [7] MATSUBAYASHI K., MAKI M., TSUZUKI T., NISHIOKA T. and SATO N.K., *Nature (London)*, **420** (2002) 143.
- [8] RHYEE J.-S. and CHO B.K., *J. Appl. Phys.*, **95** (2004) 6675.
- [9] MAITI K., MEDICHERLA V.R.R., PATIL S. and SINGH R.S., *Phys. Rev. Lett.*, **99** (2007) 266401.
- [10] MEDICHERLA V.R.R., PATIL S., SINGH R.S. and MAITI K., *Appl. Phys. Lett.*, **90** (2007) 062507.
- [11] ETOURNEAU J., MERCURIO J.-P., NASLAIN R. and HAGENMULLER P., *J. Solid. State Chem.*, **2** (1970) 332.
- [12] LOFLAND S.E., SEAMAN B., RAMANUJACHARY K.V., HUR N. and CHEONG S.W., *Phys. Rev. B*, **67** (2003) 020410(R).
- [13] BLAHA P., SCHWARZ K., MADSEN G.K.H., KVASNICKA D. and LUITZ J., **WIEN2k**, *An Augmented Plane Wave + Local Orbitals Program for Calculating Crystal Properties (Karlheinz Schwarz, Techn. Universität Wien, Austria)*, (2001) ISBN 3-9501031-1-2.
- [14] WU R., PENG G., LIU L. and FENG Y.P., *Condmate/0501104*.
- [15] BOUZERAR G. and ZIMAN T., *Phys. Rev. Lett.*, **96** (2006) 207602.

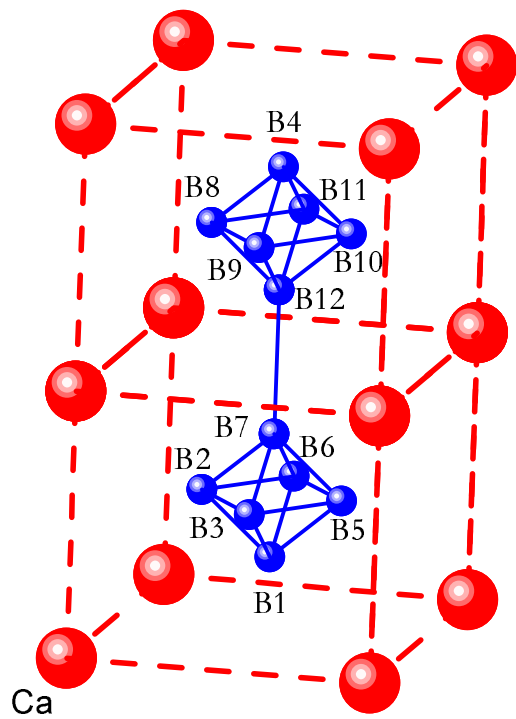


Fig. 1: (color online) The unit cell considered for the calculations containing 2 formula unit of CaB_6 . All the borons are labeled to identify the borons around the defect site. B12 is removed/replaced to introduce vacancy/impurity.

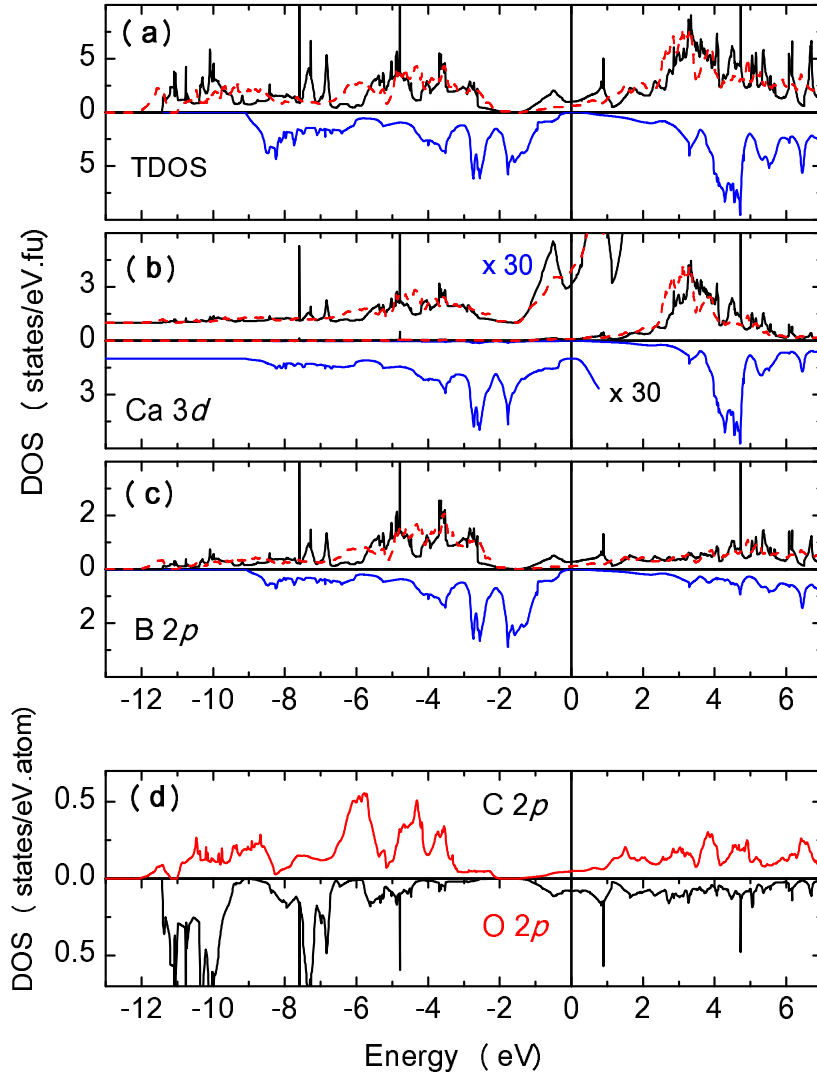


Fig. 2: (color online) Calculated (a) total density of states (TDOS) (b) Ca $3d$ partial density of states (PDOS), and (c) B $2p$ PDOS are shown. The results corresponding to CaB_6 are shown by inverted y -axis. Along the positive y -axis, $\text{CaB}_{5.5}\text{C}_{0.5}$ (dashed line) and $\text{CaB}_{5.5}\text{O}_{0.5}$ (solid line) are shown. In order to visualize Ca $3d$ PDOS in low energy region, $(\text{Ca } 3d \text{ PDOS} \times 30 + 1)$ are shown in (b). (d) C $2p$ PDOS (positive y -axis) and O $2p$ PDOS (inverted axis) for $\text{CaB}_{5.5}\text{C}_{0.5}$ and $\text{CaB}_{5.5}\text{O}_{0.5}$, respectively.

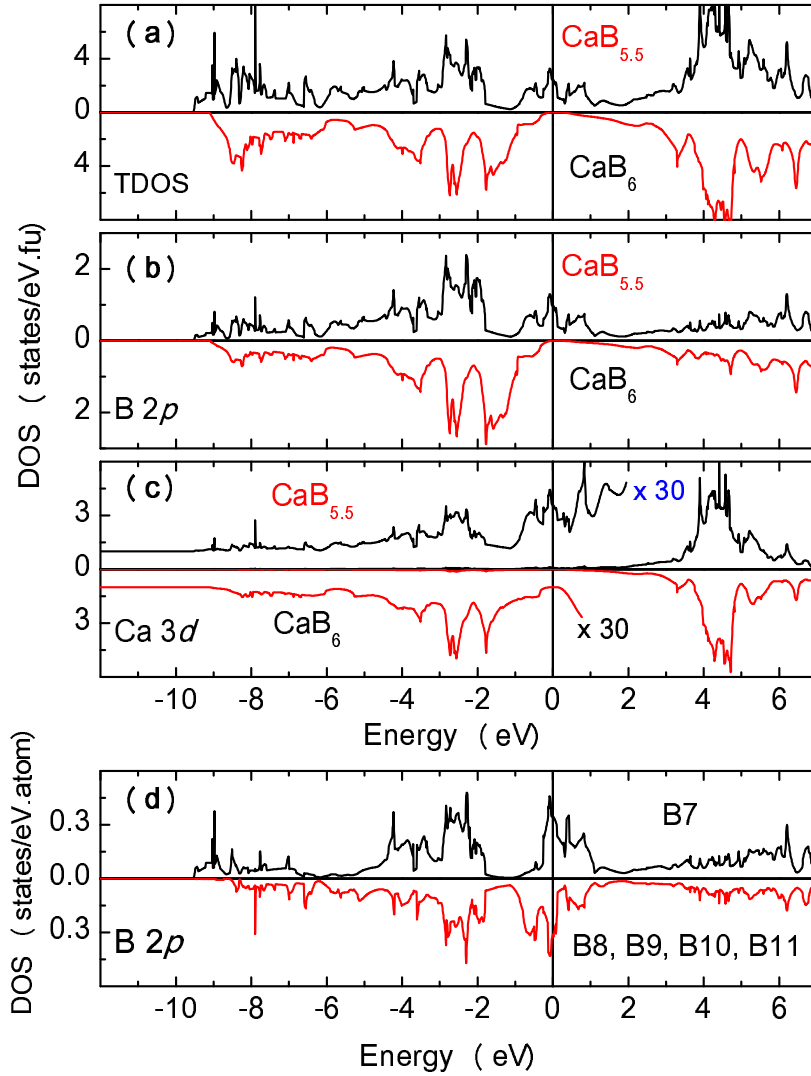


Fig. 3: (color online) Calculated (a) total density of states (TDOS), (b) B $2p$ partial density of states (PDOS), and (c) Ca $3d$ PDOS are shown. The results corresponding to CaB_6 are shown by inverted y -axis and those of $\text{CaB}_{5.5}$ are shown along the positive y -axis. In order to visualize Ca $3d$ PDOS in low energy region, Ca $3d$ PDOS $\times 30 + 1$ are shown in (c). (d) $2p$ PDOS corresponding to B7 and B8 in $\text{CaB}_{5.5}$ are shown by positive y -axis and inverted y -axis, respectively. $2p$ PDOS corresponding to B9, B10 and B11 are identical to that of B8.

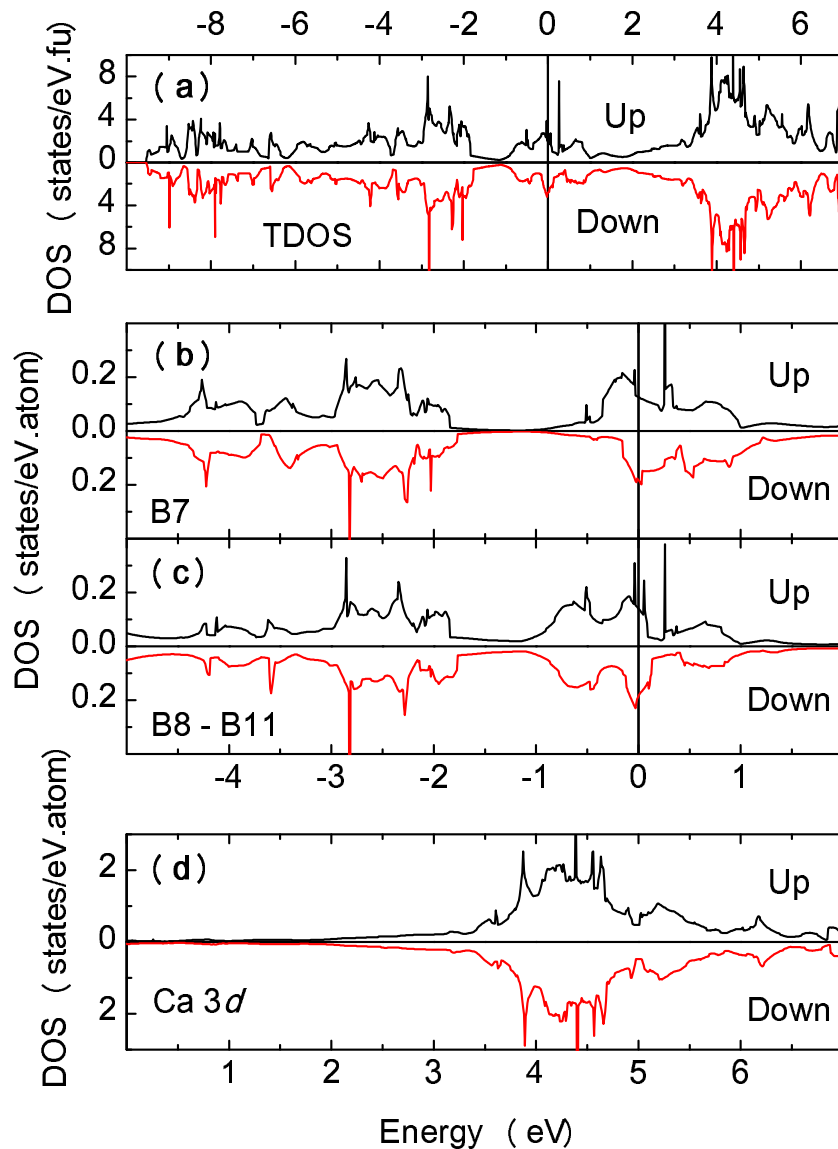


Fig. 4: (color online) Spin polarized density of states corresponding to (a) TDOS, (b) B7 $2p$ PDOS, (c) $2p$ PDOS of (B8-B11), and (d) Ca $3d$ PDOS are shown with up-spin component along positive y -axis and down-spin component along inverted y -axis. Clearly, $2p$ PDOS corresponding to B7 has the largest exchange splitting and hence large magnetic moment compared to all other borons.